Separation Science and Technology
Publication details, including instructions for authors and subscription information:
http://www.informaworld.com/smpp/title~content=t713708471

Concentration by Membrane Ultrafiltration of a Shear-Thinning Fluid

Catherine Charcosset[a]; Lionel Choplin[a]
[a] GEMICO, CENTRE DE GÉNIE CHIMIQUE DES MILIEUX COMPLEXES, NANCY CEDEX, FRANCE

To cite this Article Charcosset, Catherine and Choplin, Lionel(1995) 'Concentration by Membrane Ultrafiltration of a Shear-Thinning Fluid', Separation Science and Technology, 30: 19, 3649 — 3662
To link to this Article: DOI: 10.1080/01496399508014150
URL: http://dx.doi.org/10.1080/01496399508014150

SEPARATION SCIENCE AND TECHNOLOGY, **30**(19), pp. 3649–3662, 1995

Concentration by Membrane Ultrafiltration of a Shear-Thinning Fluid

CATHERINE CHARCOSSET* and LIONEL CHOPLIN
GEMICO, CENTRE DE GÉNIE CHIMIQUE DES MILIEUX COMPLEXES
1 RUE GRANDVILLE, BP 451, 54 001 NANCY CEDEX, FRANCE

ABSTRACT

Many commercial membrane processes involve fluids whose rheological properties are non-Newtonian. However, very little has been published on ultrafiltration of non-Newtonian fluids. The aim of this work is to show some experimental results concerning the concentration by membrane ultrafiltration of fluids whose viscosity is high and shear-thinning. Experiments were performed with xanthan solutions as model shear-thinning fluids. The variations of permeate flux with respect to the operating parameters show the unusual effects of some of these parameters. It is shown that when the feed solution in an ultrafiltration process has shear-thinning properties, those properties have an enormous influence in determining the operation efficiency.

INTRODUCTION

Many commercial membrane processes involve fluids whose rheological behavior is non-Newtonian or, more particularly, shear-thinning, e.g., the concentration by reverse osmosis of fruit juices (1, 2) and egg white (3), and the concentration by ultrafiltration of fruit juices (4), skim milk (5), and polysaccharide gums (5, 6). In other cases, e.g., whey protein (7) and mineral slurry (8), the pseudoplastic properties develop at the high concentrations which occur in the boundary layer at the membrane interface.

* To whom correspondence should be addressed at LAGEP, Université Lyon 1, 43 Bd du 11 Novembre 1918, Bat 305, 3e étage, 69 622 Villeurbanne Cedex, France.

The bulk of research into mass transfer in ultrafiltration has been performed upon bovine serum albumin or dextran solutions, both of which are Newtonian even at concentrations of the order of the wall concentration. Very little has been published on ultrafiltration of non-Newtonian fluids.

The aim of this work is to study the ultrafiltration of highly viscous fluids with shear-thinning properties. Experiments are performed with xanthan solutions as model shear-thinning fluids. The variations of permeate flux with respect to time, transmembrane pressure, axial velocity, bulk concentration, temperature, and membrane properties are discussed, showing the unusual effect of some of these parameters. The optimization of the concentration by membrane ultrafiltration of a shear-thinning fluid is discussed.

ULTRAFILTRATION MODELS

Concentration Polarization Model

Ultrafiltration is a liquid–liquid separation process of macromolecules with diameters in the 10–500 Å range. The driving force is a mechanical pressure P_{tm} applied between the two faces of the membrane.

Concentration polarization is the term used to describe the accumulation of membrane-rejected solute in a polarized layer at the membrane interface. When solutes are retained by the membrane, they accumulate in the boundary layer at a rate proportional to the permeate flux J and the solute concentration C. The accumulation creates a concentration difference which induces a diffusive flux of solutes from the wall toward the bulk fluid. A steady state is reached when convective and diffusive fluxes balance each other.

$$JC = D\frac{dC}{dr} \tag{1}$$

where D is the diffusion coefficient and r is the position on an axis normal to the membrane. Integrating Eq. (1) through the boundary layer of thickness δ gives

$$J = \frac{D}{\delta}\log\left(\frac{C_w}{C_b}\right) = k\log\left(\frac{C_w}{C_b}\right) \tag{2}$$

The solute is assumed to be completely retained by the membrane. C_w and C_b are the wall and bulk concentrations, respectively, and k is the mass transfer coefficient.

Gel Model

Some authors have used the gel layer concept to explain the phenomenon of a limiting flux (9, 10). They considered that at a sufficiently high concentration the boundary layer reaches a solubility limit, C_g, and that a gel layer forms. Any further increase in transmembrane pressure P_{tm} results in a thickening of the gel layer, thus increasing the gel layer resistance. This counteracts the increase in P_{tm} so that the permeate flux becomes independent of the transmembrane pressure. The limiting flux is obtained by substituting C_g for C_w in Eq. (2):

$$J = k \log\left(\frac{C_g}{C_b}\right) \tag{3}$$

The semilog relationship between the limiting flux and bulk concentration is frequently observed in practice, although some exceptions have been reported (11). The gel concentration C_g is obtained by extrapolation of J versus $\log(C_b)$ plots at a zero-flux intercept. However, the proposition that C_g represents a physical, solute-specified gel concentration has been questioned (12).

Osmotic Model

Considering the high concentration difference between the boundary layer and the permeate, it has been shown that the osmotic difference, $\Delta\pi$, which develops across the membrane reduces the effective pressure (13). There is thus a lower driving force for permeation:

$$J = (P_{tm} - \Delta\pi)/\mu R_m \tag{4}$$

where μ is the fluid viscosity and R_m is the membrane resistance. Any increase in the transmembrane pressure P_{tm} serves to further increase the concentration and the osmotic pressure at the membrane interface. Again, this counteracts the increase in P_{tm} so that the flux becomes insensitive to the transmembrane pressure.

Mass Transfer Coefficient

Equations for determining the mass transfer coefficient k in terms of the operating conditions take the following general form involving Sherwood, Reynolds, and Schmidt numbers (9):

$$\mathrm{Sh} = kd_h/D = A\mathrm{Re}^x\mathrm{Sc}^y \tag{5}$$

where $\mathrm{Re} = \rho u d_h/\mu$, $\mathrm{Sc} = \mu/\rho D$, d_h is the hydraulic diameter, and ρ is the density. These relations are, for example, the Lévêque equation in

laminar flow ($x = y = 1/3$) and the Dittus and Boelter law in turbulent flow ($x = 0.875$, $y = 1/3$). However, these relations were established for nonporous walls. Experimental determinations of x in laminar flow for Newtonian fluids commonly give values greater than 1/3, and of the order of 1/2 (14).

Non-Newtonian Fluids Ultrafiltration

Many non-Newtonian fluids exhibit a complex rheological behavior which may be represented by sophisticated models. However, in order to keep the analysis free of complexities, a simple power-law model is commonly used:

$$\mu = K\dot{\gamma}^{n-1} \tag{6}$$

where $\dot{\gamma}$ is the shear rate, K is the consistency index, and n is the flow index. For $n = 1$ the fluid is Newtonian, for $n < 1$ the fluid is shear-thinning or pseudoplastic, and for $n > 1$ the fluid is dilatant.

Pritchard (11) proposed an expression for the mass transfer coefficient k which incorporates the effect of pseudoplastic behavior. This expression is a tool for understanding the increase in the mass transfer coefficient that they obtained experimentally during concentration runs of xanthan solutions. However, a discrepancy is observed between the measured and predicted mass transfer coefficient.

Aimar (5) performed an experimental study of skim milk and scleroglucan pseudoplastic solutions. He concluded that the main consequence of pseudoplastic behavior is the existence of a viscosity profile in the flow direction with low viscosities close to the membrane. This leads to better mass transfer than with a Newtonian fluid of the same viscosity at rest and to greater sensitivity to the axial velocity variations.

MATERIALS AND METHODS

Crossflow Filtration Rig

The fluids are recirculated using a positive displacement pump. An helicoidal impeller is used for mixing the fluid in the feed tank. The retentate leaving the module and the permeate are returned to the feed tank in order to maintain a constant feed concentration. The flow rate through the filtration module is monitored by a rotameter, calibrated for each polymer solution. The permeate rates are measured volumetrically. Two manometers are used to measure inlet and outlet pressures; transmembrane pressure P_{tm} is the mean of inlet and outlet pressures and it is

maintained by adjusting the backpressure on the retentate leaving the module. The measurements are performed at 20 ± 2°C.

Tubular Module

The filtration module contains one tubular ceramic membrane (Carbo-Sep, Tech-Sep). The membrane length is 1.2 m, the inlet diameter is 6 mm, and the membrane surface area is 0.022 m^2. The nominal molecular weight cut-off is 50,000 daltons. The experiments are performed with an M8 membrane whose water permeability is 330 ± 50 $L/h \cdot m^2$ at 4 bar. An M4 membrane is also tested, with the same characteristics as the M8, except that the water permeability is smaller, 170 ± 50 $L/h \cdot m^2$ at 4 bar. Before the start of each run, water permeability is measured to check the stability of the microporous membrane.

Fluids

Measurements are carried out with xanthan solutions (Keltrol T, Kelco International). The average molecular weight is 2×10^6 daltons.

Rheology

The viscosity measurements are made with a cone-plate type rotational rheometer (RFS II, Rheometrics Scientific, USA). All measurements are performed at 20°C. The reported results are mean values of three measurements.

RESULTS

Xanthan Rheology

The relationship between the viscosity and the shear rate for various xanthan concentrations is shown in Fig. 1. The plots are nonlinear. At sufficiently high and low shear rates all pseudoplastic solutions cease to shear-thin and approach Newtonian viscosities. The power-law parameters, n and K in Eq. (6), are calculated from the plots in the shear-thinning region by nonlinear least-squares regression (Table 1). We observed that the flow index n decreases with increasing concentration and that the consistency index K is greatly dependent on the concentration and increases with increasing concentration.

Permeate Flux versus Time

Permeate flux drops to a steady-state value after a few minutes for fouling experiments in which transmembrane pressure and axial velocity

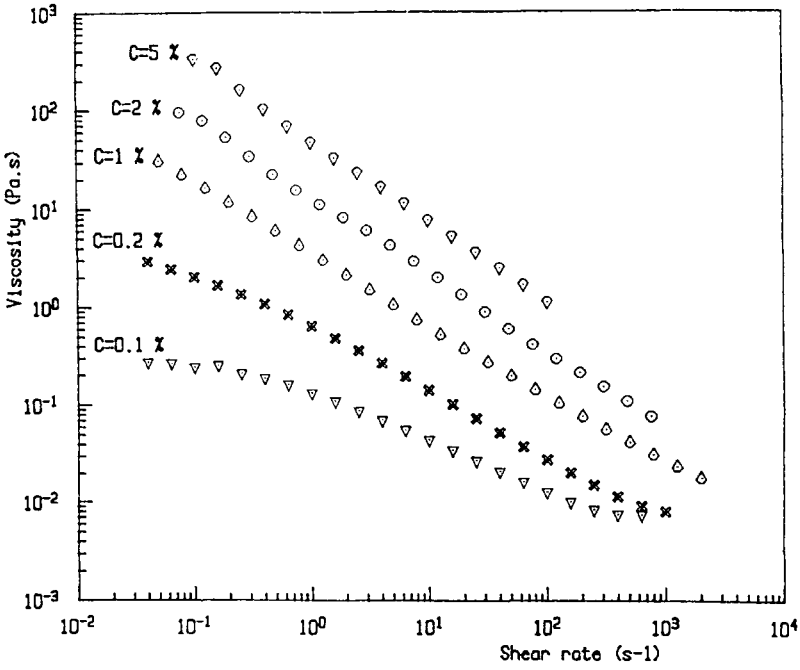

FIG. 1 Viscosity versus shear rate for xanthan solutions at various concentrations.

TABLE 1
Power Law Parameters for Xanthan Solutions. The Range of Shear Rate Covered by the Model is $\dot{\gamma}_{min} - \dot{\gamma}_{max}$

Concentration (wt%)	K (Pa·s^n)	n	$\dot{\gamma}_{min}$ (s^{-1})	$\dot{\gamma}_{max}$ (s^{-1})
0.1	0.14	0.48	1.58	157.9
0.2	0.67	0.31	1.58	100
1	3.50	0.25	1.26	79.6
2	10.94	0.24	47.5	753.7
5	56.04	0.15	3.98	100

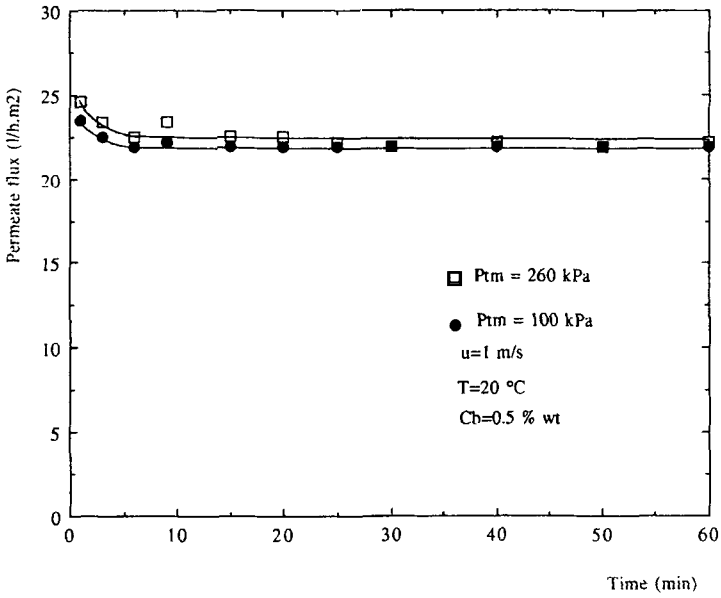

FIG. 2 Effect of the time on the permeate flux.

are constant. The permeate flux is plotted versus time in Fig. 2. Steady states are obtained after 3 minutes. This suggests that the fouling of the ultrafiltration membrane by xanthan molecules is nearly negligible under our operating conditions.

Permeate Flux versus Transmembrane Pressure

The permeate flux is plotted versus the transmembrane pressure in Fig. 3. Permeate fluxes are independent of the applied transmembrane pressure beyond 100 kPa, whatever the axial velocity. This observation suggests that the polarization phenomenon plays an important role in solvent transfer under our operating conditions, and that the role of the membrane pore structure is minimized.

Permeate Flux versus Axial Velocity

The steady-state fluxes were measured for various xanthan concentrations at decreasing axial velocity (Fig. 4). The flow is laminar as a consequence of the range of axial velocities and viscosities covered. We observed that log(permeate flux) increases in proportion to log(axial

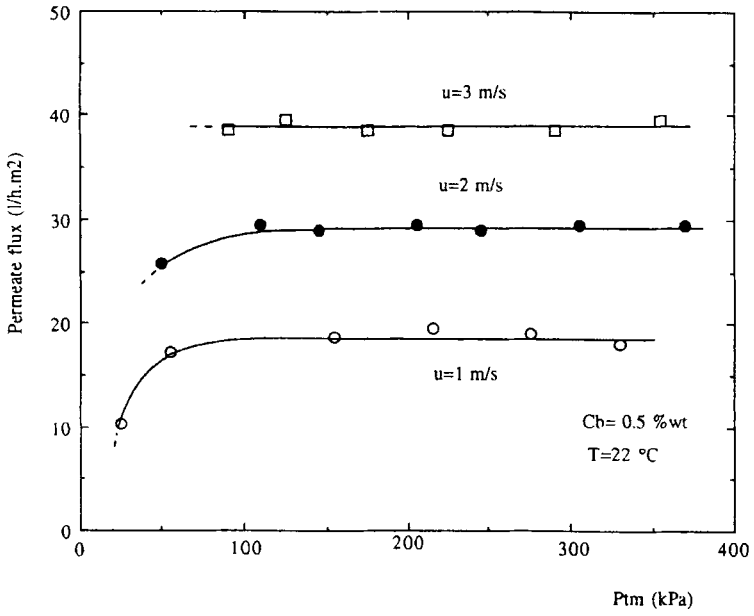

FIG. 3 Effect of the transmembrane pressure on the permeate flux.

velocity) for all concentrations. The power law parameters A and x in Eq. (7) are obtained by nonlinear least-square regression of the plots:

$$J = Au^x \tag{7}$$

The resulting correlations are shown in Table 2. The fit to the data is very good, with correlation coefficients between 0.95 and 0.99.

The axial velocity exponent is not equal to 1/3 as predicted by the Lévêque equation for Newtonian fluids and laminar flow conditions. It increases at low concentrations (from 0.59 at 0.1 wt% to 0.68 at 0.2 wt%) and decreases at larger concentrations (from 0.68 at 0.2 wt% to 0.31 at 2 wt%).

Permeate Flux versus Bulk Concentration

The plots of permeate flux versus log(bulk concentration) at constant axial velocity are shown in Fig. 5. They are obtained from the correlations listed in Table 2. The plots are different from the linear decline in flux predicted by Eq. (2) with a constant mass transfer coefficient. The decrease in J is linear only at high bulk concentration. The concentration

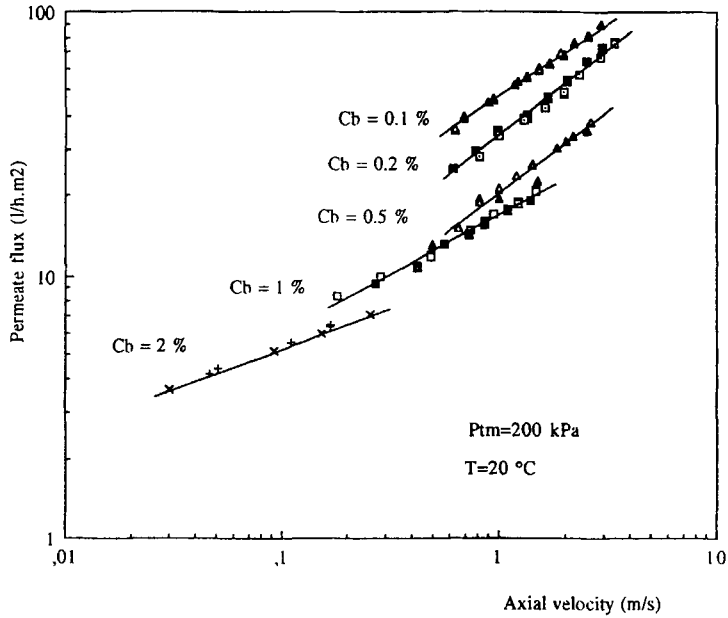

FIG. 4 Effect of the axial velocity on the permeate flux.

TABLE 2
Permeate Flux Versus Axial Velocity Regressions. The Range of Axial Velocity Covered by the Model is $u_{min} - u_{max}$

Concentration (wt%)	A^a	x^a	u_{min} (m/s)	u_{max} (m/s)
0.1	47.33	0.60	0.64	1.90
0.1	47.74	0.58	0.69	3.53
0.2	34.35	0.67	0.62	3.34
0.2	32.30	0.68	0.82	3.38
0.5	20.83	0.63	0.65	2.59
0.5	19.59	0.62	0.5	2.5
1	17.08	0.43	0.18	1.48
1	16.70	0.45	0.27	1.38
2	11.24	0.32	0.030	0.26
2	10.65	0.30	0.046	0.17

[a] With J (L/h·m^2) and u (m/s).

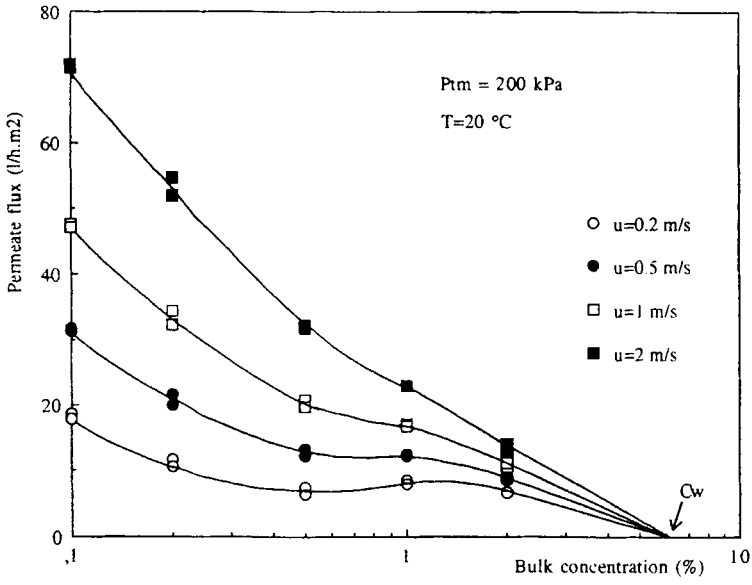

FIG. 5 Effect of the bulk concentration on the permeate flux.

at the membrane wall C_w is then determined using Eq. (2). From the intercept with $J = 0$, we obtain $C_w = 6$ wt%. The mass transfer coefficient is then calculated. We observed that it decreases at low xanthan concentration and increases at a larger concentration. For a shear-thinning fluid, the mass transfer coefficient is not constant but varies with the bulk fluid rheological properties.

Permeate Flux versus Temperature

We performed experiments where the temperature was increased from 20 to 50°C and then decreased. The variation in permeate flux versus temperature is plotted in Fig. 6. A increase in permeate flux due to higher temperature was observed because the viscosity of xanthan solutions is constant in this temperature range. The increase in permeation rate flux with temperature may be explained by the decreasing filtrate viscosity. Darcy's law predicts an increase in permeate flux close to 50% between 20 and 50°C as the filtrate (water) viscosity is decreased from 1.002 to 0.547 mPa·s.

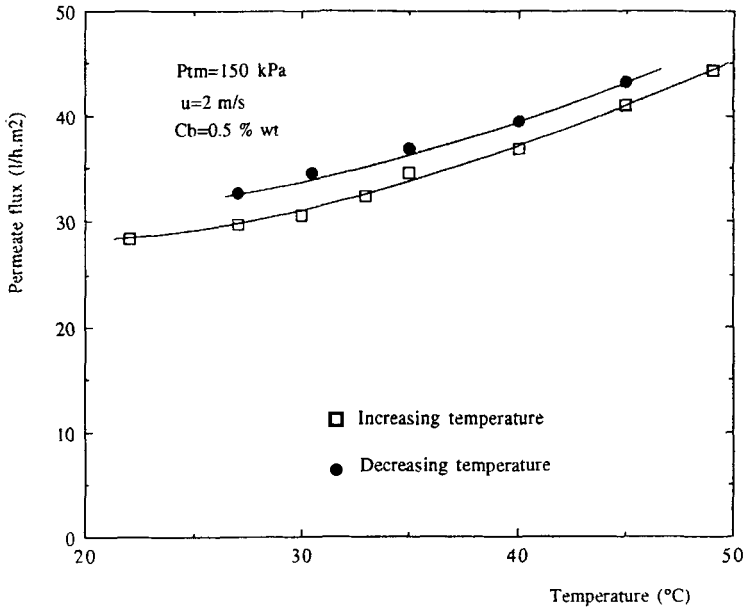

FIG. 6 Effect of the bulk fluid temperature on the permeate flux.

Permeate Flux versus Permeability

Experiments were carried out with an M4 CarboSep membrane which has the same characteristics as the M8 used previously except that the water permeability is smaller. We can see in Table 3 that the permeation flux was nearly the same in spite of large differences in initial and final permeabilities. This suggests again that the polarization phenomena plays an important role in the solvent transfer under our operating conditions

TABLE 3
Effect of the Membrane Permeability on the Permeate Flux.
P_{tm} = 150 kPa, u = 2m/s, C_b = 0.5 wt%

Membrane	M4	M8
Permeability before UF (L/h·m^2)	172.5	346.1
UF permeate flux (L/h·m^2)	25.7	27.2
Permeability after UF (L/h·m^2)	172.5	294.8

and that the membrane filtration step is nearly negligible. We can conclude that for this kind of fluid, the permeability of a given membrane of specific geometry and material has very little effect on the permeate flux under conditions of high polarization.

CONCLUSION

This work has shown some experimental results concerning the concentration by ultrafiltration of highly viscous and shear-thinning fluids. High viscosity implies high degrees of concentration polarization. Under these conditions, the role of the membrane pore structure is minimized. The permeate flux becomes independent of the transmembrane pressure beyond very low pressure (<100 kPa for our experimental conditions) and the membrane permeability has very little effect on the permeate flux. However, the permeate flux is strongly dependent on the permeate (water) temperature.

The shear-thinning properties of a fluid concentrated by membrane ultrafiltration have a strong influence in determining the operation efficiency. A consequence is the dependence of permeate flux on axial velocity varying with concentration. Therefore, it is required to measure the dependence of permeate flux on axial velocity for different bulk concentrations, as in Fig. 4. For low concentrations we observed a strong influence of axial velocity on permeate flux. Thus, it is better to feed these solutions at high velocity to get high permeate flux. High concentration solutions show little axial velocity effect on permeate flux. It is thus possible to decrease the axial velocity with only a small change in ultrafiltration efficiency.

Another consequence of the the shear-thinning properties of the fluid is the nonlinearity of the plot of J versus log(bulk concentration). Careful use of the gel model Eq. (3), commonly used for Newtonian fluids, is then suggested. The determination of the concentration at the membrane wall C_w by the intercept of the plot of J versus $\log(C_b)$ at $J = 0$ requires linearity of this plot near $J = 0$.

ACKNOWLEDGMENTS

We thank M. Cueille and M. Liou from Tech-Sep for supplying us with membranes, and Dr. Dodds and Prof. Leclerc for their help in providing part of the experimental set-up. Financial support provided by the Centre National de la Recherche Scientifique (CNRS) and the sponsoring companies of the Gemico laboratory [Elf-Atochem, Lafarge Coppee, Michelin,

Rhône-Poulenc Industrialisation, Gray-Valley (Total)] is gratefully acknowledged.

SYMBOLS

C	concentration of solute
d_h	hydraulic diameter of membrane (m)
D	diffusion coefficient of solute (m^2/s)
J	permeate flux through membrane (m/s or $L/h \cdot m^2$)
k	solute mass transfer coefficient (m/s)
K	consistency index ($Pa \cdot s^n$)
n	flow behavior index
P_{tm}	transmembrane pressure drop (kPa)
r	radial position (m)
R_m	membrane resistance (m^{-1})
T	temperature (°C)
u	axial velocity (m/s)

Greek Symbols

$\dot{\gamma}$	shear rate (s^{-1})
μ	viscosity (Pa·s)
δ	thickness of the boundary layer (m)
ρ	density (kg/m^3)
$\Delta\pi$	osmotic pressure difference across the membrane (kPa)

Subscripts

b	bulk
g	gel
w	wall/membrane fluid interface

REFERENCES

1. K. Ishii, S. Konomi, K. Kojima, and M. Kai, "Development of a Tomato Juice Concentration System by Reverse Osmosis," in *Synthetic Membranes: HF and UF Uses*, American Chemical Society, 1981, pp. 5–16.
2. D. Pepper, A. C. J. Orchard, and A. J. Merry, "Concentration of Tomato Juice and Other Fruit Juices by Reverse Osmosis," *Desalination*, *53*, 157–166 (1985).
3. E. Lowe, E. L. Durkee, R. L. Merson, K. Ijichi, and S. L. Cimino, "Egg White Concentrated by Reverse Osmosis," *Food Technol.*, *23*, 45–54 (1969).
4. R. L. Thomas, J. L. Gaddis, P. H. Westtfall, T. C. Titus, and N. D. Ellis, "Optimization of Apple Juice Production by Single Pass Metallic Membrane Ultrafiltration," *J. Food Sci.*, *52*, 1263–1266 (1987).

5. P. Aimar, "Ultrafiltration of Pseudoplastic Fluids," in *Separations for Biotechnology* (M. S. Verrall and M. J. Hudson, Eds.), Ellis Horwood, Chichester, UK, 1987, pp. 360–372.
6. A. Haarstick, U. Rau, and F. Wagner, "Cross-Flow Filtration as a Method of Separating Fungal Cells and Purifying the Polysaccharide Produced," in *5th World Filtration Congress*, Nice, France, June 1990, pp. 342–347.
7. G. Jonsson, "Boundary Layer Phenomena during Ultrafiltration of Dextran and Whey Protein Solutions," *Desalination*, *51*, 61–77 (1984).
8. M. R. Hoogland, C. J. D. Fell, A. G. Fane, and D. A. R. Jones, "The Optimum Design of Crossflow Filtration Elements for Mineral Slurry Processing," in *5th World Filtration Congress*, Nice, France, 1990, pp. 604–610.
9. W. F. Blatt, A. Dravid, A. S. Michaels, and L. Nelsen, "Solute Polarization and Cake Formation in Membrane Ultrafiltration: Causes, Consequences, and Control Techniques," in *Membrane Science and Technology*, (J. E. Flinn, Ed.), Plenum Press, New York, 1970, pp. 47–97.
10. A. S. Michaels, "New Separation Technique for the CPI," *Chem Eng Prog.*, *64*, 31–43 (1968).
11. M. Pritchard, "The Influence of Rheology upon Mass Transfer in Cross-Flow Membrane Filtration, Ph.D. Thesis, University of Bath, 1990.
12. K. Isaacson, P. Duenas, C. Ford, and M. Lysagh, "Determination of Graetz Solution Constants in the In-Vitro Hemofiltration of Albumin, Plasma and Blood," in *Ultrafiltration Membranes and Applications* (A. R. Cooper, Ed.), Plenum Press, New York, 1980, pp. 507–522.
13. J. Wijmans, S. Nakao, V. D. Berg, F. Troelstra, and C. Smolders, "Hydrodynamic Resistance of Concentration Polarization Layers in Ultrafiltration," *J. Membr. Sci.*, *22*, 117–135 (1985).
14. M. Lopèz-Leiva, "Prediction of Permeate Fluxes in UF/RO Systems," in *Ultrafiltration Membranes and Applications* (A. R. Cooper, Ed.), Plenum Press, New York, 1980, pp. 269–282.

Received by editor April 4, 1995